01 Aug 2014

Theoretical/experimental Comparison of Deep Tunneling Decay of Quasi-bound H(D)OCO to H(D) + CO_2

Albert F. Wagner

Richard Dawes
Missouri University of Science and Technology, dawesr@mst.edu

Robert Continetti

Hua Guo

Recommended Citation

A. F. Wagner et al., "Theoretical/experimental Comparison of Deep Tunneling Decay of Quasi-bound H(D)OCO to H(D) + CO_2," *Journal of Chemical Physics*, vol. 141, no. 5, American Institute of Physics (AIP), Aug 2014.
The definitive version is available at https://doi.org/10.1063/1.4891675

Theoretical/experimental comparison of deep tunneling decay of quasi-bound H(D)OCO to H(D) + CO_2

Albert F. Wagner,[1,a)] Richard Dawes,[2] Robert E. Continetti,[3] and Hua Guo[4]
[1]*Chemical Sciences and Engineering Division, Argonne National Laboratory, Lemont, Illinois 60439, USA*
[2]*Department of Chemistry, Missouri University of Science and Technology, Rolla, Missouri 65409, USA*
[3]*Department of Chemistry and Biochemistry, University of California, San Diego, California 92093, USA*
[4]*Department of Chemistry and Chemical Biology, University of New Mexico, Albuquerque, New Mexico 87131, USA*

(Received 9 April 2014; accepted 18 July 2014; published online 5 August 2014)

The measured H(D)OCO survival fractions of the photoelectron-photofragment coincidence experiments by the Continetti group are qualitatively reproduced by tunneling calculations to H(D) + CO_2 on several recent *ab initio* potential energy surfaces for the HOCO system. The tunneling calculations involve effective one-dimensional barriers based on steepest descent paths computed on each potential energy surface. The resulting tunneling probabilities are converted into H(D)OCO survival fractions using a model developed by the Continetti group in which every oscillation of the H(D)-OCO stretch provides an opportunity to tunnel. Four different potential energy surfaces are examined with the best qualitative agreement with experiment occurring for the PIP-NN surface based on UCCSD(T)-F12a/AVTZ electronic structure calculations and also a partial surface constructed for this study based on CASPT2/AVDZ electronic structure calculations. These two surfaces differ in barrier height by 1.6 kcal/mol but when matched at the saddle point have an almost identical shape along their reaction paths. The PIP surface is a less accurate fit to a smaller *ab initio* data set than that used for PIP-NN and its computed survival fractions are somewhat inferior to PIP-NN. The LTSH potential energy surface is the oldest surface examined and is qualitatively incompatible with experiment. This surface also has a small discontinuity that is easily repaired. On each surface, four different approximate tunneling methods are compared but only the small curvature tunneling method and the improved semiclassical transition state method produce useful results on all four surfaces. The results of these two methods are generally comparable and in qualitative agreement with experiment on the PIP-NN and CASPT2 surfaces. The original semiclassical transition state theory method produces qualitatively incorrect tunneling probabilities on all surfaces except the PIP. The Eckart tunneling method uses the least amount of information about the reaction path and produces too high a tunneling probability on PIP-NN surface, leading to survival fractions that peak at half their measured values. © *2014 AIP Publishing LLC*. [http://dx.doi.org/10.1063/1.4891675]

I. INTRODUCTION

The elementary reaction OH + CO → H + CO_2 is of great important in hydrocarbon combustion and atmospheric chemistry. In combustion, the reaction represents the main heat release step.[1] In the terrestrial atmosphere, the reaction is a major sink for the hydroxyl radical.[2] In the atmosphere of Venus, the reaction plays a key role in the cycling of CO_2.[3] While strongly exothermic, the reaction features a very stable intermediate, HOCO, and a barrier to activation in the product channel of roughly similar energy to the reactants.[4] As a consequence, the thermal rate constants for this reaction show significant non-Arrhenius behavior.[5] The exact height and shape of the barrier to the formation of H + CO_2 are critical to the overall kinetics of the reaction.

Because of its importance, this reaction has been the subject of a vast number of experimental studies that have recently been reviewed.[6] These studies are dominated by thermal kinetics measurements. Until recently, *direct* measurements of the properties of the HOCO radical consisted of a few limited spectroscopic studies.[7–13] However, a new approach involving photoelectron-photofragment coincidence (PPC) measurements starting from the H(D)OCO^- anion has become available.[14–16] In these experiments, the unimolecular decay of a neutral H(D)OCO radical by tunneling to H(D) + CO_2 can be directly observed. Of course all the thermal kinetics measurements have contributions of tunneling in them but there is no definitive way from only the measurements themselves to isolate and characterize the tunneling contribution. Furthermore, only tunneling processes near the top of the barrier are able to compete with non-tunneling processes in thermal reaction rates. The PPC measurements are not done on thermalized HOCO radicals and are primarily sensitive to deep tunneling. These measurements will be described in more detail in Sec. II.

Since the OH + CO reaction has only four atoms, it is quite amenable to theoretical study and numerous such studies have been done.[6] The considerable majority of these studies have used statistical reaction rate theory of various forms

a)Author to whom correspondence should be addressed. Electronic mail: wagner@anl.gov

applied to reaction path characterizations of the potential energy surface (PES) in order to obtain thermal reaction rates to compare to the thermal kinetics measurements. Several global representations of the PES have been developed.[17–24] Two of these PES have been explicitly used in comparison to the PPC measurements. The LTSH PES[19] was unfavorably contrasted[16] to an adjustable potential optimized to reproduce measured tunneling of H(D)OCO to H + CO_2. The PIP PES, which was previously denoted as the CCSD-3/d PES,[21] was used in full and reduced dimensionality quantum dynamics calculations[25] of the dissociation process. Reasonably good agreement was made with experiment, although the cost of the calculations limited the extent of the comparison to experiment. This PES was also used in classical trajectory calculations of the OH + CO reaction[26,27] and the reverse H + CO_2 reaction.[21] The computed fractions of translational, vibrational, and rotational energy disposal in the CO_2 product are noticeably different from experiment. Approximate quantum dynamics calculations[28] were also applied to an early version of this PES to obtain reaction rates that were somewhat too low at low temperatures and too high at high temperatures. The newest PES,[24] called PIP-NN, increases by ∼50% the number of *ab initio* points in its fit over those used in the PIP PES. However, the same classical trajectory and approximate quantum dynamics calculations used for PIP PES studies produce on PIP-NN very similar results that remain at odds with experiment. This surface has recently been used to compute mode specific tunneling probabilities modeling the PPC experiment.[29] In this paper, we will use the LTSH, PIP, and PIP-NN PESs to examine deep tunneling in comparison to the PPC measurements. In addition we will use a calculated reaction path based on the CASPT2 electronic structure method.[30] This calculation was done for this study and represents an exploration of the impact that multi-reference flexibility in the electronic structure calculations can have on HOCO PES features.

As mentioned above, quantum dynamics wavepacket calculations in 5D and 6D have been done on both the PIP and PIP-NN PESs. These calculations are too expensive to be propagated long enough to allow an extensive comparison to PPC measurements. However, in reporting the PPC measurements, Johnson *et al.*[16] also develop a model that converts a computed tunneling probability for a 1D effective potential into directly measured HOCO survival fractions from the time of their creation to their arrival more than 7 μs later at the detector. In a similar way, thermal rate constant calculations typically do not incorporate tunneling based on a full-dimensional quantum dynamics calculation but rather on an approximate calculation involving some kind of representation of the reaction path. These approximate calculations on the PESs listed above can produce deep tunneling probabilities that can be incorporated into the Johnson *et al.* model to produce survival fractions for direct comparison to the measured ones.

There are three approximate tunneling methods widely used for thermal tunneling that can be in principle used for the deep tunneling processes of importance here. The oldest is the Eckart method based on an analytic quantum dynamics solution[31] to a three-parameter 1D barrier potential. Probably the most widely used tunneling method for thermal kinetics is the small curvature tunneling (SCT) method embodied in the software POLYRATE.[32] The third method is the semiclassical transition state theory (SCTST) method developed originally by Miller *et al.*[33] and embodied in the Multiwell program suite.[34] Recently an improvement of this method was developed[35] that is specific to deep tunneling and is denoted iSCTST. Missing from this list of tunneling methods is the Wigner tunneling method;[36] it is based on a parabolic representation of the reaction barrier which is too approximate for deep tunneling. The four other tunneling methods enumerated above will be used in the comparison to experiment.

The rest of this article is as follows. Section II will briefly review the PPC experiment and describe the model of Johnson *et al.* that converts tunneling probabilities into the observed survival fractions. Section III will review and contrast the four different PESs and the four different approximate tunneling methods discussed above. Section IV will discuss the resulting tunneling probabilities and then compare for each PES the calculated and measured survival probabilities. Section V will summarize what has been learned by the comparison of experiment and theory.

II. PHOTODETACHMENT EXPERIMENT AND MODEL

The Continetti group has extensively reported[14–16] photoelectron-photofragment coincidence (PPC) spectroscopy for HOCO and DOCO. As the *cis* isomer of the anion has a lower energy, the neutral HOCO/DOCO produced by photodetachment is dominated by the *cis* isomer. Hence, all discussions below will be referred to this isomer if not indicated explicitly. In the final version of the experiment, the initially created anions are cooled and stored in a cryogenic linear electrostatic ion beam trap. Photodetachment at a fixed wavelength of the cooled anions and measurement of the electron kinetic energy (eKE) allows determination of the internal energy of the metastable neutral. The neutral molecule travels for microseconds down a translational spectrometer whose detector at the end measures the center-of-mass translational energy release in coincidence with the photoelectron. Such measurements detect the tunneling of H(D)OCO to H(D) + CO_2 that has occurred during the time of flight. The reported results for the survival fraction F of H(D)OCO in the face of this tunneling process is shown and repeated in each of the three panels of Fig. 1 as a function of eKE.

The survival fraction was analyzed with a model that connects tunneling probability P through a 1D effective barrier to the survival fraction F. The primary relationship is

$$F(E_{int}) = (1 - P(E_{int}))^N, \quad (1)$$

where E_{int} is the internal energy of the H(D)OCO and N is the number of classical oscillations of frequency ω (in cm^{-1}) of H(D)-OCO in HOCO that occur during the time of flight t_{TOF}:

$$N = t_{TOF}\omega c, \quad (2)$$

where c is the speed of light. In this model, HOCO gets an opportunity to tunnel at every outer turning point of the H–OCO stretch. Because a t_{TOF} of 7.8 μs for HOCO and

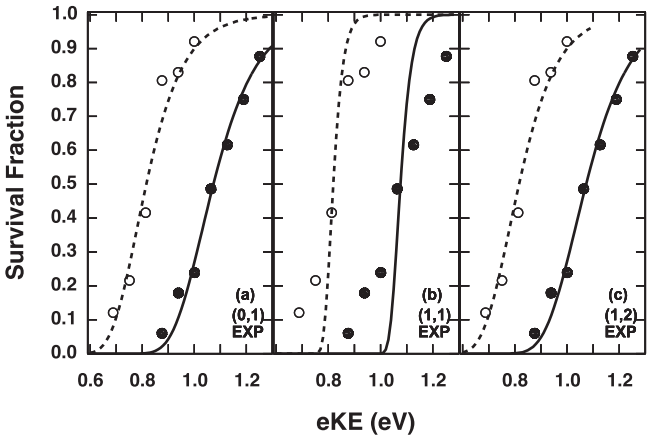

FIG. 1. Survival fraction as a function of eKE as measured (solid symbols for HOCO and open symbols for DOCO) and as calculated (solid lines for HOCO and, dashed lines for DOCO) for the adjustable model potential for three different initial vibrational quantum numbers for H(D)-OCO stretch. See text for details.

7.9 μs for DOCO is very long on a molecular timescale, N is a number measured in hundreds of millions for either isotope. This means that this experiment is sensitive to the very small probabilities that occur in deep tunneling.

An effective 1D potential in an effective tunneling coordinate dominated by H–OCO stretch is assumed. This implies that only a part of E_{int} is aligned with the tunneling coordinate. If E_{diss} is the aligned energy, then the model assumes

$$E_{diss} = E_{OH(D)}(\nu_{max}) + \chi[E_{int} - E_{OH(D)}(\nu_{max})], \quad (3)$$

where $E_{OH(D)}(\nu_{max})$ is the anharmonic vibrational energy in the H(D)-OCO stretch mode at the dominant vibrational quantum number ν_{max}. This approximation basically says that all the energy in the H(D)-OCO stretch and some fraction χ of the rest of the energy is aligned with the effective tunneling coordinate and contributes to tunneling through the barrier. The parameters ν_{max} and χ are unknown and are adjusted to optimize agreement with experiment. In principle both ν_{max} and χ are isotope dependent but the actual application of this model to the experiments used a common value χ but isotopically different values for ν_{max}. In the context of this model, E_{int} is connected to eKE by

$$E_{int} = h\nu - (AEA - zpe_{OH(D)} - eKE), \quad (4)$$

where $h\nu$ is the photon energy used in the photodetachment, AEA is the adiabatic electron affinity of HOCO, and $zpe_{OH(D)}$ is the zero point energy for the H(D)-OCO stretch. The zpe correction in Eq. (4) ensures that E_{diss} is measured from the base of the effective 1D potential which includes the zero point energy of all HOCO modes *except* H(D)-OCO. In principle, E_{int} should be quantized and thus has only discrete values. This implies through Eq. (4) that eKE should be discrete. However, the measurements at this relatively high photon energy do not resolve the discrete nature of eKE which in turn means this model will represent survival fractions as continuous functions of eKE.

This model was applied along with an adjustable effective 1D barrier and a WKB formula for tunneling through the barrier. Optimization of the adjustable barrier to maximize the agreement with experiment produced the lines in Fig. 1 for the three possible values of (ν_{max}[HOCO], ν_{max}[DOCO]) indicated in each panel of the figure. For each panel, the optimized potential is noticeably different with barriers ranging from 26.1 kcal/mol to 35.8 kcal/mol (see Sec. 1 of the supplementary material of this article for details of the optimized potential).[51] Only panel (c) for ν_{max} = (1,2) was published and discussed (in Ref. 16 and its supplementary material). Panel (c) in Fig. 1 is slightly different from the published results because of improvements in the model detailed in the Sec. 1 of the supplementary material.[51] These improvements concern a more internally consistent treatment of anharmonicity in the H(D)-OCO stretch and updated experimental constants like adiabatic electron affinities. These improvements apply to all calculated survival fractions in this article.

In Sec. IV, we will apply the same model but derive effective 1D barriers directly from the four PESs listed in Sec. I. The results will be reported in figures analogous to Fig. 1 only the same effective potential will be used for all three panels instead of being optimized for each panel as in Fig. 1. In anticipation of these results, four features of Fig. 1 merit comment:

- In panel (c), the computed results terminate for DOCO and HOCO at an eKE value less than the maximum in the plot. In the model, the departing electron must leave at least enough energy to populate the selected initial H(D)-OCO vibrational states. That caps the eKE that is possible, leading to a termination of computed results for panel (c) at $E_{int} = E_{OH(D)}(\nu_{max})$. Since this termination depends only on the value of ν_{max}, panels (b) and (c) share the same ν_{max} for HOCO and thus the same termination of the computed results. In panel (b) this termination is obscured by the DOCO survival fraction that does not terminate over the range of energies in the plot. Higher values of ν_{max} than those used in the figure, i.e., (1,2), are not acceptable because the termination would occur at values of eKE above which there are measured values of survival fractions. All plots of survival fractions in this article will have this termination feature. At the cap of eKE, the tunneling probability is the smallest it can be because E_{diss} is at a minimum. This in turn means that the survival fraction is the maximum it can be as a function of eKE. If a potential is relatively easy to tunnel through, then the higher values of $E_{OH(D)}(\nu_{max})$ will become unsatisfactory because the computed survival fractions will be below measurements and no optimization in χ will be able to corrected it.
- The middle panel is in qualitatively poorer agreement with experiment than the other two panels. This panel is for the only combination of ν_{max} where the energy in the D-OCO stretch is *less* than the energy in the H–OCO stretch. The optimization process of the model produces χ = 1.0, which from Eq. (3) means that HOCO and DOCO have the identical and maximum energy available for dissociation at a common eKE. The model adjusts the potential to get the correct

displacement in eKE of the HOCO and DOCO survival fraction but does not have enough flexibility to get a large enough range of eKE over which survival fractions go from 0 to 1.

- The optimized value of χ for panel (a) is larger (0.32) than that for panel (c) (0.19). Lower $E_{OH(D)}(v_{max})$ for panel (a) is in part compensated in E_{diss} by a higher value of χ.
- As pointed out by Johnson *et al.*,[16] the difference between E_{int} and E_{diss} represents internal energy not used in the tunneling process and can be thought of as the internal energy the product CO_2 is initially created with as it appears on the other side of the barrier. At the completion of the tunneling process, the H + CO_2 system is initially on a repulsive wall of the potential. While most of this repulsive potential energy will largely go into the translational energy with which H and CO_2 will separate from each other, some fraction may perhaps be converted into internal energy of CO_2. This makes $E_{int} - E_{diss}$ a reasonable lower bound on the internal energy of the CO_2 product. The average product internal energy was measured by Johnson *et al.* at 0.2 eV for HOCO and 0.3 eV for DOCO. It is easy to show from Eq. (3) that

$$E_{int} - E_{diss} = [E_{int} - E_{OH(D)}(v_{max})](1 - \chi). \quad (5)$$

Since E_{int} depends on eKE, this estimate of the internal energy of CO_2 also varies with eKE and the average internal energy requires a convolution over the measured probability of eKE for the H + CO_2 product. However, tests show that that convolution is essentially the same as evaluating Eq. (4) where the computed survival fraction is 0.5. In doing this for the results in Fig. 1, the average internal energy of CO_2 for the calculations in all three panels is about the same for HOCO and DOCO and varies as: 0.4 for panel (a), 0.0 for panel (b), and 0.2 for panel (c). The 0.0 value for panel (b) is an automatic consequence of $\chi = 1.0$, implying all of E_{int} is used to tunnel. Considering this model may underestimate the internal energy of CO_2, panel (c) for $v_{max} = (1,2)$ makes the best contact with experiment, is the most consistent with the basic assumption that dissociation is promoted by energy in the H–OCO stretch, and was the only panel originally published by Johnson *et al.*

In Sec. III, the theoretical methods used to develop four *ab initio* multidimensional potentials for HOCO and reduce them to tunneling probabilities will be described. In Sec. IV, the methods developed in this completed section will then be applied to these tunneling probabilities to produce survival fractions for comparison to experiment.

III. THEORETICAL METHODS

A. Potential energy surfaces

The four PESs listed in Sec. I will now be described in more detail.

The LTSH[19] PES is the oldest of the four. It is composed of a switched together set of local representations of the PES where each local representation is fit to potential energies calculated by electronic structure methods that differ from local region to local region. While this PES was successfully used to produce some of the first credible calculated descriptions of both the kinetics and dynamics of the OH + CO ↔ H + CO_2 system, in its original form[37] it is not directly suitable for this application to deep tunneling. As detailed in Sec. 2 of the supplementary material,[51] the LTSH reaction path for the tunneling process of interest is discontinuous on the HOCO side of the saddle point. The small (∼0.1 kcal/mol) discontinuity occurs because a switch that mixes together two different representations of the potential is abruptly turned off when the value of the switch falls out of a finite range. The actual version of the LTSH potential used, which will be denoted LTSH1, simply suppresses the turn off. As discussed in the supplementary material, this results in little change to the PES other than to remove the discontinuity.[51]

In both LTSH and LTSH1, there is an additional difficulty of interpretation of the PES. In the published description of the PES[19] and in comment cards within the LTSH code,[37] the saddle point connecting the *cis*-HOCO and H+CO_2 is said to have a *cis* geometry. While this is true for the underlying electronic structure calculations, the saddle point is *trans* on the fitted surface. On the LTSH1 PES, the steepest descent reaction path leads to the *trans*-HOCO. At equilibrium, the *cis*-HOCO and *trans*-HOCO are separated by an out-of-plane saddle point. On either fitted PES, progress along the *trans* reaction path eventually causes the *cis* form to become the *maximum* in the potential experienced during out-of-plane motion. Consequently all attempts to find a *cis* saddle point failed. Although this disagrees with all substantial electronic structure calculations, the reaction path on the LTSH1 will be used in this article as is and that fact that it is *trans* will be ignored.

The PIP PES is the third and last of a series of three PESs,[26] based on increasing numbers of better located potential energies calculated with the UCCSD(T)-F12b/AVTZ level of theory[38,39] and fit with the permutation invariant polynomial (PIP) method of Bowman and co-workers.[40] In this version, 53 000 *ab initio* potential energies up to 100 kcal/mol above the *trans*-HOCO equilibrium are incorporated into the fit. The rms error of the fit is 0.86 kcal/mol.

The PIP-NN PES uses a neural network (NN) fit[41,42] to 74 443 potential energy calculated with the UCCSD(T)-F12a/AVTZ level of theory with full permutational invariance. This is essentially the same *ab initio* method used for PIP but applied to the calculation of more potential energies. For energies less than ∼70 kcal/mol, the rms error of the fit is 0.07 kcal/mol, about an order of magnitude improvement over the fitting error for PIP. The maximum error is 2.9 kcal/mol. An earlier version[23] of this PES had comparable fitting errors but imperfect permutational invariance; it was used in a recent model of the mode specific HOCO tunneling.[43]

The CASPT2 data calculated for this study was part of an exploration of the use of multi-reference electronic structure methods for the HOCO system. In a global PES, such methods are more flexible in representing the many different and evolving bonding configurations, including for HOCO, at and between the HCO_2, *cis* and *trans* HOCO and van der Waals bonded OH-CO structures. Given a large enough active space, multi-reference methods can smoothly transition between

regions where a particular configuration is dominant. There are some HOCO geometries at which single reference methods cannot be converged or are unreliable. To avoid including poor data in a single-reference based PES generally one must try to identify points with excessive multi-configurational character by some approach such as the T_1 diagnostic.[44] If the regions without data coverage are too large, then it becomes difficult to obtain a well-behaved and well-determined fit. A T_1 diagnostic threshold was used to exclude points in the UCCSD(T) based PESs mentioned above, but for HOCO this represented a small fraction of the total data set and no obvious issues arose from lack of coverage.[21,26] MRCI calculations with large active spaces are extremely expensive for the HOCO system relative to UCCSD(T) calculations with the same basis set and predict fairly similar relative energies for the various critical points. One previously noted difference is that a presumably correct C_{2V} geometry is obtained for the HCO_2 minimum by multi-reference methods whereas a slightly skewed C_s structure is obtained with UCCSD(T).[26] Complicated electronic structure and multistate effects have been noted in this region[26,45] and for some purposes a multistate description would be warranted, but the features most relevant to the current study occur on the ground state and are the relative energies of the minima and the heights and widths of the barriers between them. Determining the reaction path using POLYRATE/MOLPRO requires several Hessian and numerous gradient calculations which were determined to be prohibitively expensive at the MRCI/CBS and full-valence (17e,13o) active space level. The CASPT2 method (which provides analytic gradients) was tested, but was found to greatly overly stabilize both *cis* and *trans* HOCO isomers (relative to OH + CO) when used with large basis sets and a full-valence active space. However, tests found that (presumably due to cancelation of errors) the relatively inexpensive CASPT2/AVDZ method using a reduced (13e,11o) active space reproduces some features of much more expensive MRCI/CBS calculations.

For this work, MOLPRO[46] was used to characterize the following the regions of the PES:

- The *cis*- and *trans*-H(D)OCO and CO_2 equilibrium regions at the harmonic level.
- The saddle point region at the complete cubic and partial quartic level necessary to carry out a second order vibrational perturbation theory calculation.
- The description of the reaction paths for H(D)OCO → H(D) + CO_2 under the direction of a POLYRATE/MOLPRO combined code.[47]

This level of characterization of the PES is sufficient for all four tunneling methods mentioned in the introduction. From this portion of the PES, one can compute $\Delta H_{rxn}(0°K)$ for HO + CO → H + CO_2. At the CASPT2(13e,11o)/AVDZ level the calculated harmonic value of $\Delta H_{rxn}(0°K)$ is −24.01 kcal/mol, a few hundredths off from the ATcT experimental value[48] of −24.03 kcal/mol. For HO + CO → *cis*-HOCO, the calculated harmonic value of $\Delta H_{rxn}(0°K)$ is −23.89 kcal/mol, deeper than the ATcT value of −23.12 ± 0.20 kcal/mol by about 0.75 kcal/mol. However, for *trans*-HOCO → *cis*-HOCO, the computed harmonic value of $\Delta H_{rxn}(0°K)$ is −0.91 kcal/mol, in considerable error from the ATcT experimental value of +2.04 kcal/mol and in contrast to the three PESs above that all have *trans*-HOCO as the more stable isomer. At the CASPT2 level, the *cis*-HOCO is somewhat too stable while the *trans*-HOCO is significantly not stable enough.

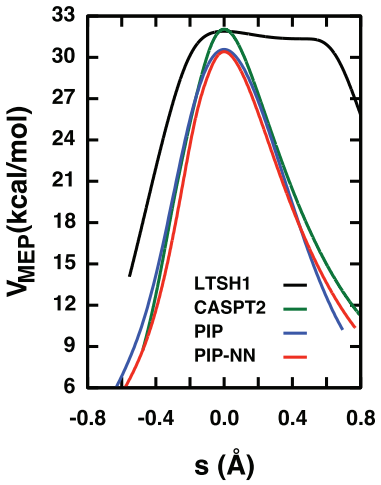

FIG. 2. V_{MEP} along the steepest descent path from the saddle point versus the reaction coordinate s. Negative(positive) s values are for the descent to HOCO(H + CO_2). Lines are color-coded for each PES as indicated. See text for details.

In Fig. 2, V_{MEP}, the energy along the minimum energy path, can be obtained as a function of s, the reaction coordinate or the progress along the path, for all four PESs. Here s = 0.0 is at the saddle point on each PES and negative (positive) values of s trace the path to HOCO (H+CO_2). The reaction path is formally different for the DOCO system but the results are only slightly different from those in Fig. 2. The zero of energy in the figure is the equilibrium of HOCO in the *cis* form for CASPT2, PIP, and PIP-NN but, as mentioned above, the *trans* form for LTSH1. The figure clearly shows that LTSH1 is an outlier with a barrier qualitatively thicker than any other PES, a point originally noted by Johnson *et al.*[16] The PIP and PIP-NN PESs have quite similar barriers, as would be expected because they are based on closely related data sets of *ab initio* potential energies. Somewhat surprisingly, the PIP-NN PES is generally, but not always, noticeably thinner than the PIP. The CASPT2 barrier is the highest of the four PESs at 32.0 kcal/mol. Alone among the four PESs, the *cis*-HOCO is *lower* than the *trans*-HOCO and part of the exceptional barrier height may be this over estimation of the stability of the *cis* isomer. If the CASPT2 curve in Fig. 2 is shifted down to match at the saddle point the PIP-NN curve, there is a near perfect superposition of the two curves except at the very lowest energies in the figure (see Sec. 2 of the supplementary material for more details).[51] At those lowest energies, the PIP-NN curve tails off to a higher energy *cis*-HOCO while the CASPT2 continues to plunge to a lower energy *cis*-HOCO.

The results in Fig. 2 can be considered an approximation to a 1D tunneling path.[49] However, the five degrees of freedom perpendicular to that path are not accounted for. If one assumes an adiabatic model for those five degrees of freedom

and corrects the results in Fig. 2 for the change in the zero point energy as a function of s for those five degrees of freedom, an effective 1D tunneling path is produced. This path through the model of Johnson *et al.* can then be processed to produce survival fractions for comparison to experiment. All four tunneling methods used in this article carry out this basic approach in different ways as will be detailed next.

B. Tunneling methods

As mentioned previously, exact quantum dynamics has been carried out on a number of PESs based on UCCSD(T) data. However, such calculations cannot feasibly carried out to characterize tunneling over the microseconds required to make contact with experiment. In the spirit of the original experimental model, four different approximate tunneling methods are used to estimate tunneling on each of the four PESs. These four approximations are the Eckart approximation, semiclassical transition state theory as represented in the software package MULTIWELL and labeled SCTST, improved SCTST (iSCTST) which is a recent correction to SCTST appropriate for deep tunneling, and the semiclassical transmission coefficient in the small curvature limit as represented in the software package POLYRATE and labeled SCT.

Like the original experimental model, all four of these methods take as input an effective one-dimensional barrier potential through which HOCO reactants must tunnel to the $H + CO_2$ products. This one-dimensional potential is zero-point corrected along its whole length for the five degrees of freedom perpendicular to the reaction coordinate. Conceptually at least, that reaction coordinate at the HOCO reactant at equilibrium is assumed to be the vibrational mode most dominated by H atom motion relative to nearest O atom. At the top of the barrier, the process of determining the saddle point on each one of the PESs determines the reaction coordinate.

Each of the four approximate tunneling methods differs in the construction of the effective one-dimensional barrier and in the solution of the tunneling dynamics given the barrier. In the order first listed:

Eckart: This is an exact quantum dynamics solution[31] to an analytic potential with three adjustable parameters that reproduce the zero-point corrected barriers in the forward and reverse direction and the imaginary frequency at the saddle point. Informed of the actual PES by only these three parameters, this method requires the least detailed characterization of the PES. However, unlike the other methods that are all based on semiclassical dynamics, the dynamics here is done exactly quantum mechanically.

SCTST: This is an exact semiclassical dynamics solution[33] to an effective potential as defined by a second order vibrational perturbation theory (VPT2) description of the saddle point. Such a description is full dimensional, producing a vector of frequencies defining the harmonic curvature of the potential at the saddle point, and a matrix, called the x matrix, of second order anharmonic corrections. The resulting potential in the vicinity of the saddle point can be thought of as a multidimensional Morse Oscillator in which for the reaction coordinate direction the Morse Oscillator potential is inverted producing a barrier through which tunneling can occur. With a sum-of-states approach and this potential, an elegant and analytic solution to the exact semiclassical dynamics is available. VPT2 uses up to and including multidimensional fourth derivatives of the PES at the saddle point and therefore informs this tunneling approach with more detail about the actual PES. There are operational details about this method as applied to the HOCO tunneling problem that are described in Sec. 3 of the supplementary material.[51]

iSCTST: For a bound 1D Morse Oscillator, the frequency ω_e, the anharmonic correction $x_e\omega_e$, and the dissociation energy D_e are related so that knowing any two of these quantities gives you the third. Similarly, for SCTST, knowing the vector of frequencies and the x matrix from VPT2 at the saddle point gives the effective dissociation energy or, in the case of the tunneling coordinate, the effective barrier height of the inverted Morse Oscillator for that coordinate. However, any second order theory about the saddle point is typically insufficient to give a quantitatively correct and, in many cases, qualitatively correct forward and reverse reaction barriers. These barriers are determined from calculations done at the reactant and product asymptotes that are apart from the VPT2 calculations at the saddle point. As a consequence, for *deep* tunneling, SCTST can have serious errors. iSCTST[35] creates an effective one-dimensional potential that reproduces all VPT2 characteristics at the saddle point and in addition reproduces the correct forward and reverse barriers. Furthermore, for this particular potential the classical action is analytic and, as in SCTST, can be directly converted into a semiclassical tunneling probability. This HOCO tunneling study represents one of the first applications of iSCTST beyond model problems. Details of its implementation are described in Sec. 3 of the supplementary material.[51]

SCT: In this approach, a reaction path Hamiltonian is constructed based on a rigorous, steepest descent description of the reaction path in both directions from the saddle point. This approach incorporates the most information from the actual PES. Formally, a complete reaction path Hamiltonian is difficult to numerically solve for the semiclassical action that leads to the tunneling probability. However, in various limits, such as the small curvature limit used here, the semiclassical action can be reduced to various integrals that can be conveniently and reliably solved using the numerical machinery in POLYRATE.[32] Other limits, such as the large curvature limit, can also be reduced to stable numerical integrations but tests showed that the small curvature limit was most appropriate (as discussed in the supplementary material).[51]

Although the SCT approach incorporates the most information from the actual PES, there are two reasons why the SCT one-dimensional potential may not be the best for this particular application. First, the definition of the reaction path and its zero-point correction for the one-dimensional potential depends on the coordinates used. The product OCO is a linear molecule with a doubly degenerate bend but nowhere else on the reaction path is there such symmetry. As is discussed in Sec. 3 of the supplementary material,[51] there is no consistent set of coordinates for the whole reaction path flexible enough to describe the evolution of this symmetry, resulting in imperfect zero-point corrections near the base of the barrier.

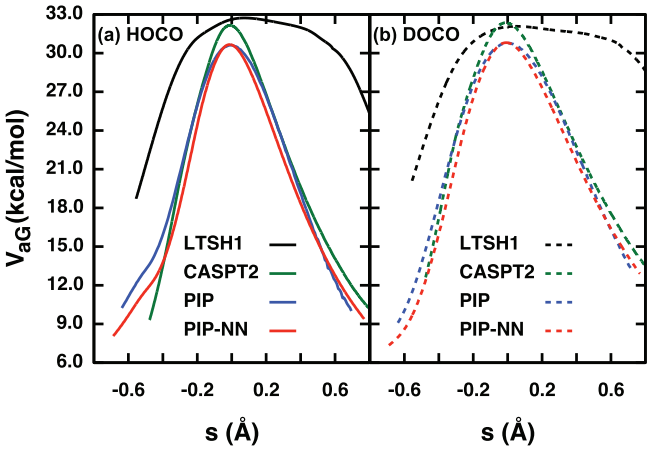

FIG. 3. The zero-pointed corrected effective one-dimensional potentials V_{aG} versus the reaction coordinate s for HOCO (a) and DOCO (b). Lines are color-coded for each PES as in Fig. 2. See text for details.

Second, it is well known[50] that a mathematically steepest descent path approaches an equilibrium position on the PES along a reaction coordinate that coincides with the lowest frequency equilibrium normal mode direction. In the case of HOCO this would correspond to an O–C–O bending type motion. Unfortunately the experimental model that will convert the computed tunneling probability into experimentally measured quantities expects that reaction coordinate for the one-dimensional potential to have an H–O stretch character. As discussed in Sec. III, the encroachment of H–O stretch character in perpendicular modes of motion as the reaction path approaches reactants causes an increase in the zero-point correction near the base of the barrier that is inconsistent with the experimental model.

In Fig. 3, the zero point energy corrected effective one-dimensional potentials for both HOCO (panel (a)) and DOCO (panel (b)) are displayed as calculated by POLYRATE where this quantity is called V_{aG}. For both panels, the zero of energy is the equilibrium H(D)OCO potential plus the zero-point for the five degrees of freedom that are not dominated by the H(D)-OCO stretch. At the broadest level of comparison, both panels in Fig. 3 are similar to each other and similar to the uncorrected potentials seen in Fig. 2. At a higher level of detail, there are three additional observations. First, the flare-out on the reactant side seen for PIP and PIP-NN in panel (a) is the manifestation of an H–OCO character invading the zero-point correction as discussed above. This is not so evident in panel (b) for DOCO because the absolute size of the zero-point energy is smaller. For CASPT2 and LTSH1 PESs, this effect is there but not so exposed over the range plotted in the figure. This thickening of the HOCO effective barrier first becomes noticeable about 15 kcal/mol below the reaction barrier and thus affects only the deepest tunneling. Second, LTSH1 is unique in two ways. Unlike the other three PESs, the location of the zero-point corrected barrier is noticeably displaced from the saddle point. The uncorrected potential in Fig. 2 is quite flat in the region of the barrier allowing minor changes in frequencies to shift the zero-pointed correct barrier in Fig. 3. Uniquely among the PESs, for LTSH1 the DOCO barrier on the effective one-dimensional potential is noticeably *lower* than the analogous HOCO barrier. This requires that, for the five non-(H–OCO) degrees of freedom included in the effective potential, the deuteration-induced lowering in zero-point energy at the equilibrium has to be smaller than the analogous lowering at the saddle point. Normally at the saddle point one expects the zero-point energy for conserved degrees of freedom to be somewhat smaller relative to the reactant and thus deuteration effects to be smaller also. Uniquely for LTSH1, the zero-point energy of the five degrees of freedom is *higher* at the saddle point than at equilibrium and thus deuteration effects are larger. Given an effective potential lower for DOCO than HOCO, at energies near the top of the DOCO barrier, D will tunnel through a shorter enough effective barrier than that for H to paradoxically have a higher tunneling probability. The third and last observation is the very similar shape of the CASPT2 and PIP-NN effective potentials if the CASPT2 PES is shifted down in energy to match the effective barrier on the PIP-NN PES. This is a continuation of their similarity in Fig. 2 for the potential without zero-point correction and is developed in more detail in Sec. 2 of the supplementary material.[51]

To summarize the tunneling methods, SCT has a one-dimensional effective potential most informed by the PES but imperfectly matched to the Johnson *et al.*[16] model and SCT solves its dynamics in the small curvature limit. Eckart, SCTST, and iSCTST have increasing PES content in their one-dimensional potential but still much less than SCT. However, their dynamics, quantum or semiclassical, are solved with more rigor.

IV. RESULTS

The tunneling probabilities on each of the four PESs are described immediately below in Sec. IV A. These probabilities are converted by the model into survival fractions for direct comparison to experimental measurements in Sec. IV B.

A. Tunneling probabilities

Figure 4 displays on four panels for the four different PESs the application of the four different tunneling methods to produce tunneling probabilities as a function of energy for both HOCO and DOCO. The plotted range of probabilities encompasses all that is relevant to the experimentally measured survival fractions that will be discussed in Sec. IV B. The zero of energy is that used for the effective one-dimensional potentials of Fig. 3, namely the H(D)OCO equilibrium potential energy plus the zero-point energy of the five degrees of freedom that are not dominated by the H(D)-OCO stretch. The results in Fig. 4 are not quite comprehensive because the SCTST DOCO tunneling probabilities are not plotted to ease congestion.

At the broadest level of comparison, Fig. 4 shows, not surprisingly, that the LTSH1 results are qualitatively different from the other three PESs. The thickness of the LTSH1 PES makes the probabilities drop very rapidly as the energy falls below the barrier. The flat top to the barrier makes

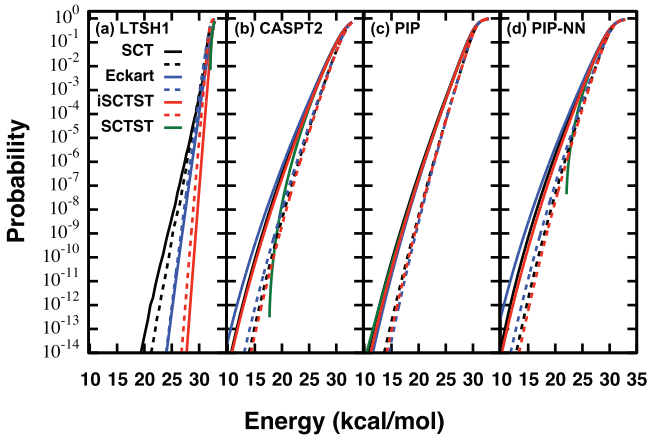

FIG. 4. Tunneling probability for HOCO (solid lines) and DOCO (dashed lines) as a function of energy for four different color-coded tunneling methods. Each of four PESs is as labeled in the four panels. See text for details.

tunneling based on variable amounts of saddle point information (Eckart, SCTST, and iSCTST) grossly different from each other and from the SCT method that uses the full reaction path. It also makes the SCTST method terminate at energies just a kcal/mol below the effective barrier where the method incorrectly locates the base of the effective potential. The lower effective barrier for DOCO versus HOCO makes for DOCO tunneling probabilities that exceed that of HOCO for energies very near the top of the barrier.

In contrast, the results for the CASPT2, PIP, and PIP-NN are largely qualitatively similar in the general shape of the tunneling probability as a function of energy and in the echoing of method ordering from HOCO to DOCO. Only in the behavior of the SCTST tunneling are these three PESs qualitatively different. As discussed in Sec. III, starting from the saddle point on each PES (see Fig. 2), the SCTST method locates the base of the effective potential well above that of the zero of energy in Fig. 4 for CASPT2 and PIP-NN but well below the zero of energy for PIP. Consequently the green line for SCTST HOCO tunneling probability terminates when this base is reached (as is also true for LTSH1 in Fig. 4). This results in an odd shape of the tunneling probability as a function of energy that causes it to stand out from all the other methods. In contrast, for PIP with a base below the zero of energy, the SCTST results for HOCO can barely be distinguished from the SCT results over the whole range of the plot. (Of course, had the plot been extended to negative energies, SCTST would uniquely still produce a finite but very small tunneling probability.) The SCTST DOCO results not present in Fig. 4 echo the SCTST HOCO results.

At a finer level of detail, the three PESs do have different tunneling characteristics. The CASPT2 and PIP-NN tend to have higher tunneling probabilities at the same energy than those of PIP. Both CASPT2 and PIP-NN have at the same energy an ordering from high to low of Eckart, SCT, and iSCTST in the deep tunneling region with Eckart being clearly higher. As indicated with respect to Figs. 2 and 3 and in Sec. 2 of the supplementary material,[51] the CASPT2 and PIP-NN have the same shape to V_{MEP} and V_{aG} if the CASPT2 results are shifted down in energy to match the PIP-NN results at the saddle point. As a consequence, the CASPT2 probabilities at a shifted higher energy are quite similar to the PIP-NN probabilities at an un-shifted energy if the shift is that to align V_{aG} for the two PESs (see Sec. 2 of the supplementary material for further details).[51] In contrast, PIP and PIP-NN have in Fig. 3 the same effective barrier height, allowing without any shift a direct comparison of PIP and PIP-NN in panels (c) and (d). Unlike PIP-NN, PIP has a different ordering of SCT, iSCTST, and Eckart with all three being clumped relatively close together.

iSCTST was developed to correct the deep tunneling flaws for SCTST and the results in Fig. 4 are one of its first realistic applications. iSCTST does behave in a qualitatively correct manner over the energy range of the plot for all four PESs. For CASPT2, PIP, and PIP-NN, iSCTST is quite close to SCT, closer than Eckart is. For LTSH1, Eckart is closer to SCT than iSCTST but, as discussed above, there are many features of LTSH1 that are anomalous. As discussed previously, iSCTST has different but generally less PES content than SCT and is therefore typically less expensive to obtain.

B. Survival fraction

Given the tunneling probabilities in Fig. 4 and the model in Sec. II the survival fraction for HOCO and DOCO can be computed as a function of electron kinetic energy (eKE). Because the SCTST method is qualitatively flawed for deep tunneling on most of the PESs, it will not be used to compute survival fractions. The model has two adjustable parameters: the initial H(D)-OCO vibrational state and the fraction χ of remaining internal energy that can be used to assist the tunneling. The parameter values can be optimized to maximize agreement with experiment. The range of eKE sampled in the experiment make only three combinations of initial H(D)-OCO vibrational quantum numbers possible: (0,1), (1,1), (1,2) where the first number is for H–OCO and the second number is for D-OCO. In the results to follow, survival fractions for each of these three combinations are displayed. For each combination only χ is optimized. While, in principle χ can be isotope dependent, for most of the results to follow the same χ was used for both isotopes as was the case for the original application of the model to an adjustable potential discussed in Sec. II. The effect of optimizing χ separately for HOCO and DOCO will be discussed at the end of this section.

For LTSH1, the optimized computed survival fraction as a function of eKE is displayed in Fig. 5 with the optimized values of χ listed in Table I. The experimental results are the solid (HOCO) and open (DOCO) symbols while the solid (HOCO) and dashed (DOCO) curves are computed using Eckart, iSCTST, and SCT color coded as in Fig. 4. The figure is analogous to Fig. 1 except that the same effective 1D potential is used in each panel and multiple tunneling methods are used in each panel. The results in the figure show the LTSH1 PES is incompatible with the measurements. Because the LTSH1 PES is so thick, small changes in the energy make very large changes in the probability no matter what tunneling method is used. This means the energy range over which the computed survival fraction goes from 0 to 1 is much narrower

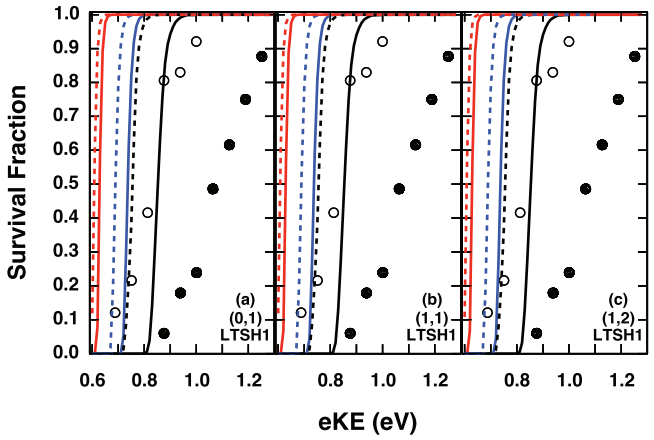

FIG. 5. Survival fraction as a function of eKE as measured (solid symbols for HOCO and open symbols for DOCO) and as calculated (solid lines for HOCO and dashed lines of DOCO) for three different initial vibrational quantum numbers for H(D)-OCO stretch on the LTSH1 PES. Different curves correspond to different tunneling methods using the color code of Fig. 4. See text for details.

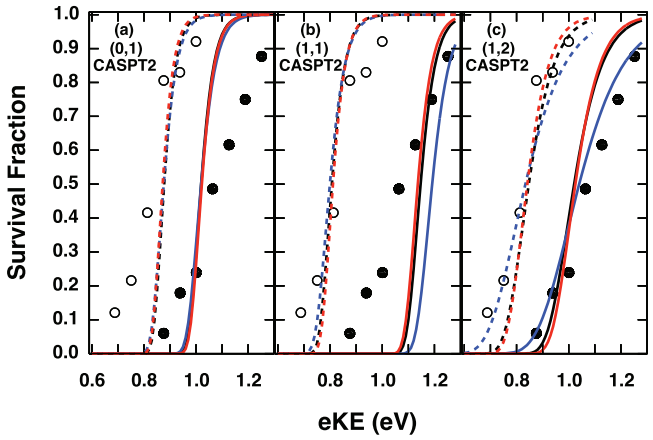

FIG. 6. As in Fig. 5 only for CASPT2.

than experiment. The thick barrier also means only tunneling energies near the top of the barrier can lead to zero survival. High tunneling energies correspond to low values of eKE, resulting in survival fraction changes all taking place at far lower values of eKE than that measured. Table I shows that the results in Fig. 5 are for an optimized value of χ that is 1.0, a physically unrealistic value that means that the departing electron leaves all internal energy in H(D)OCO directed along the tunneling coordinate. From Eq. (5) this results in a product CO_2 with no internal energy, in contrast to experimental measurements of 0.2–0.3 eV. The original application of the model with an adjustable potential also concluded that the LTSH PES has a profile along the reaction path too dissimilar to the optimized potential to be consistent with experiment. The results in Fig. 5 completely support that observation.

For CASPT2, the optimized computed survival fraction as a function of eKE is displayed in Fig. 6 with the optimal value of χ listed in Table I. The computed results in Fig. 6 make qualitative contact with experiment. The width of the eKE region where the survival fraction for either isotope goes from 0 to 1 monotonically increases from panel (a) to panel (c). The eKE region width is most like experiment in panel (c) but still too narrow. The separation in eKE space of the survival fraction for DOCO and HOCO is smallest for panel (a), largest for panel (b), and intermediate for panel (c). Again panel (c) is most like experiment but the separation is still too small. The optimal value of χ in Table I decreases monotonically from panel (a) where $E_{OH}(v_{max}) + E_{OD}(v_{max})$ is smallest to panel (c) where $E_{OH}(v_{max}) + E_{OD}(v_{max})$ is largest. This same trend was mentioned for panels (a) and (c) in Fig. 1. To illustrate this behavior more quantitatively, consider the eKE value 1.064 eV where the measured HOCO survival fraction is closest to 0.5. Across the panels, the range in $E_{OH}(v_{max})$ is about 9.3 kcal/mol but at eKE = 1.064 eV, the range of E_{diss} from Eq. (3) using the SCT χ values in Table I is 1.93 kcal/mol. In others words, the optimal value of χ reduces the variation in E_{diss} to one fifth the variation in $E_{OH}(v_{max})$ across the panels. With Eq. (5) and with the same procedure as described for Fig. 1, the lower bound estimate to internal energy of CO_2 is ~0.15 eV for both HOCO and DOCO in panels (a) and (c) and ~0.1 eV (HOCO) and ~0.2 eV (DOCO) for panel (b). These results are in reasonable accord with the measured values of 0.2 eV(HOCO) and 0.3 eV(DOCO).

Within each panel, the SCT and iSCTST results are quite close to each other, too close to be distinguished from each other by measurements with the precision of those given in the figure. The Eckart results in panel (b) and especially panel (c) are distinguishable from the results of the other tunneling methods. To understand the variations in the survival fraction from panel to panel, it is best to start from panel (c) and work backwards to panel (a).

In panel (c), all the survival fraction curves terminate at the maximum value of eKE consistent with $E_{OH(D)}(v_{max})$ (see the discussion for Fig. 1). The value of the survival fraction at the termination point is independent of χ and is the maximum survival fraction possible. The Eckart maximum survival fraction nearly equals the highest measured HOCO and DOCO survival fractions at nearby values of eKE. By optimizing to a relatively small value of χ, a relatively large range in eKE maps through Eqs. (3) and (4) into the relatively small range of E_{diss} that spans the survival fraction variation from 1 to 0. This leads to good agreement with experiment. From Fig. 4,

TABLE I. Optimized value of χ as a function of the tunneling method, the PES, and the initial vibrational state quantum numbers.

PES	v_{max}	SCT	Eckart	iSCTST
LTSH1	(0,1)	1.00	1.00	1.00
	(1,1)	1.00	1.00	1.00
	(1,2)	1.00	1.00	1.00
CASPT2	(0,1)	0.74	0.69	0.76
	(1,1)	0.65	0.60	0.68
	(1,2)	0.34	0.23	0.39
PIP	(0,1)	0.73	0.77	0.75
	(1,1)	0.64	0.68	0.66
	(1,2)	0.33	0.41	0.38
PIP-NN	(0,1)	0.64	0.58	0.68
	(1,1)	0.55	0.50	0.58
	(1,2)	0.15	0.03	0.22

SCT and iSCTST have lower tunneling probabilities than Eckart has, leading to noticeably higher maximum HOCO survival fractions than measured while the maximum DOCO survival fraction remains consistent with measurement. To compensate for the too high maximum HOCO survival fraction, an optimized χ value higher than that for Eckart rapidly drives down the HOCO survival fraction as eKE decreases, at the price of poorer DOCO agreement and a narrower range of eKE over which for either isotope the survival fraction goes from 1 to 0. Consequently, the SCT and iSCTST agreement with experiment is not as good as that for Eckart.

In panel (b), E_{OD} has changed by one quantum from the value used in panel (c). If the optimized χ value were to remain the same between the two panels, then the HOCO survival fraction would be the same for both panels but the DOCO survival fraction would be shifted to lower values of eKE. If eKE(c) is a particular value of eKE in panel (c), then the eKE whose E_{diss} is exactly the same as that for eKE(c) can be determined from Eqs. (3) and (4) as

$$\mathrm{eKE} = \mathrm{eKE\,(c)} - \left(\frac{1}{\chi} - 1\right)\left[E_{OD}\,(2) - E_{OD}\,(1)\right]. \quad (6)$$

For the same χ value in panel (c), the DOCO survival fraction would shift down in eKE by the second term in Eq. (6). (This is not precisely so because decreasing E_{OD} also reduces N in Eq. (2) but it is the dominant effect.) Since $E_{OD}(2) - E_{OD}(1) = \sim 0.3$ eV, any value of χ listed in Table I for panel (c) would shift the computed survival fraction to much lower values of eKE than seen in experiment. The only remedy is to optimize to a higher value of χ than in panel (c) at the price of an undershoot for the HOCO survival fraction relative to experiment and too narrow a range of eKE where the survival fraction for either isotope goes from 1 to 0.

For panel (a), E_{OH} has changed by one quantum from the value used in panel (b). A generalized version of the shift in Eq. (6) causes the HOCO survival fraction of panel (b) to shift to lower values of eKE in panel (a). This shift is smaller than between panels (b) and (c) because the values of χ involved from Table I are all greater than 0.5, making the the $(1/\chi - 1)$ factor in the shift in Eq. (6) a fraction. The shift at the χ value of panel (b) is still too large, leading to an optimization to a higher χ value at the price of primarily an undershoot of the computed DOCO survival fraction and primarily an overshoot of the computed HOCO survival fraction.

Overall, for CASPT2 panel (c) with $v_{max} = (1,2)$ makes the best contact with experiment, especially for the Eckart method. Of course, the agreement with experiment is not as good as panel (c) in Fig. 1 where the potential is adjusted to reproduce the experiment.

For PIP, the optimized computed survival fraction as a function of eKE is displayed in Fig. 7 with the optimal value of χ listed in Table I. As in Fig. 6 for CASPT2, the eKE region width over which the survival fraction goes from 0 to 1 increases monotonically from panel (a) to panel (c). In this regard, panel (c) is most like experiment. Like CASPT2, the separation of the survival fractions for DOCO and HOCO is largest for panel (b) with panel (c) being smaller and panel (a) being smallest. The general similarity of Fig. 7 to Fig. 6 and

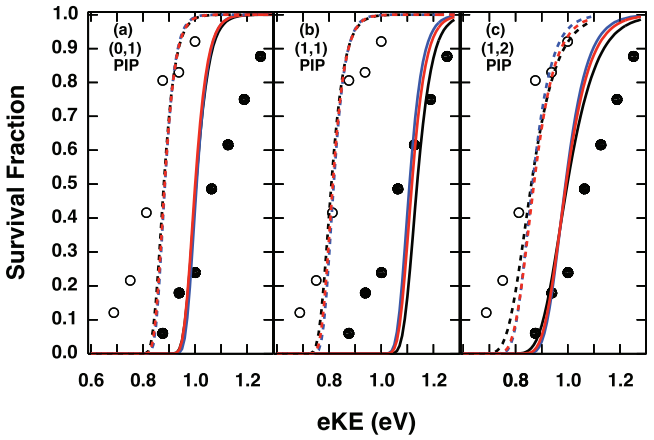

FIG. 7. As in Fig. 5 only for PIP.

of optimal χ values for PIP and CASPT2 as listed in Table I lead to the same lower bound estimate to internal energy of CO_2: ~0.15 eV for both HOCO and DOCO in panels (a) and (c) and ~0.1 eV (HOCO) and ~0.2 eV (DOCO) for panel (b), all in reasonable accord with the measured values.

The variation of the computed survival fraction from panel to panel in Fig. 7 can be understood in the same manner as the variation in Fig. 6. The two primary differences between the PIP and CASPT2 results derive from (1) the Eckart tunneling probability is not substantially different from that for SCT or iSCTST and (2) the HOCO (but not DOCO) tunneling probabilities for all methods are lower for PIP at the same E_{diss}. One consequence of these differences is that the Eckart computed survival fractions do not stand out for PIP as they do for CASPT2. A second consequence is that the DOCO survival fractions are nearly the same in each panel for PIP and CASPT2 but the HOCO survival fractions are somewhat higher, acting to shift the survival fraction to lower values of eKE. Overall, panel (c) makes the best contact with experiment. Relative to CASPT2, agreement with experiment is marginally worse for SCT and iSCTST and substantially worse for Eckart.

For PIP-NN, the optimized computed survival fraction as a function of eKE is displayed in Fig. 8 with the optimal value of χ listed in Table I. The most outstanding feature in Fig. 8

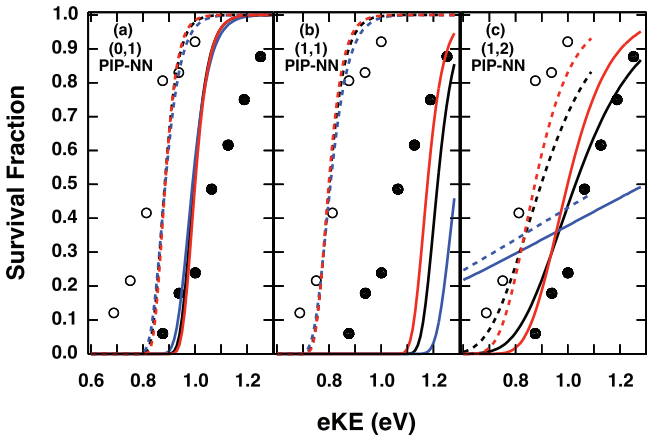

FIG. 8. As in Fig. 5 only for PIP-NN.

is the strange behavior of the Eckart probability in panel (c). The origin of this behavior is that the Eckart maximum survival fraction is a factor of two below nearby measured values. In Table I, the optimal value of χ is 0.03, just a little above zero where from Eq. (3) there would be no dependence of survival fraction on eKE. The slightly positive optimal value of χ is simply trying to make the best out of a qualitatively bad situation. From Fig. 4, the PIP-NN Eckart tunneling probability is higher in the deep tunneling regime than any other tunneling probability in the figure. It is too high to be consistent with experiment if the H–OCO quantum number is 1 as it is in panels (b) and (c).

The two other tunneling methods produce in Fig. 4 higher HOCO and DOCO tunneling probabilities than their counterparts on the PIP and CASPT2 PESs. As a consequence, in panel (c) the maximum survival fractions for both isotopes are lower than for the other PESs but not so low to significantly undershoot the measurements for both isotopes. The optimal value of χ leads to the survival fraction going from 1 to 0 over a relatively broad range of energies similar to the measurements and to the Eckart survival fractions on CASPT2. In detail, unlike the CASPT2 or PIP PESs, the DOCO maximum survival fractions for SCT and iSCTST are lower than the nearby measured values and noticeably lower than the HOCO maximum survival fraction. This results in the DOCO and HOCO survival fractions being closer together in eKE space than is measured or as found in the Eckart results on CASPT2.

The variations from panel (c) found in panels (a) and (b) of Fig. 8 are driven by the same effects discussed for Figs. 6 and 7. Overall, panel (c) makes the best contact with experiment with the exception of the Eckart computed results that are qualitatively incorrect.

In Table I, the values of χ for CASPT2 are all higher than the analogous values for PIP-NN. For the case of ν_{max} = (1,2) the CASPT2 values are about twice as big as those for PIP-NN. As mentioned in regards to Figs. 2–4 and in Sec. 2 of the supplementary material,[51] the CASPT2 effective potential has the same shape as the PIP-NN effective potential but shifted up in energy. As a consequence, the PIP-NN tunneling probability at a given E_{diss} is similar to the CASPT2 tunneling probability at a shifted higher E_{diss}. The higher CASPT2 χ values relative to PIP-NN are attempting to do that although through Eq. (3) χ cannot induce a constant shift independent of energy.

In Figures 6–8, the best agreement with experiment occurs in panel (c) for the highest quantum states in the H(D)-OCO stretch. This was also the case in the first application of the model to an adjustable potential. Within panel (c) there is sensitivity to both the PES and the tunneling method. The best results are obtained for CASPT2 with Eckart tunneling followed by PIP-NN with either SCT or iSCTST tunneling. These results are characterized by a relatively broad range of eKE over which the survival fractions change from 0 to 1 which better tracks the dependence of the measured survival fractions with eKE.

In the model applied above, χ is restricted to be the same for both isotopes. There is no inherent physical reason why this should be the case. Removing that restriction produces

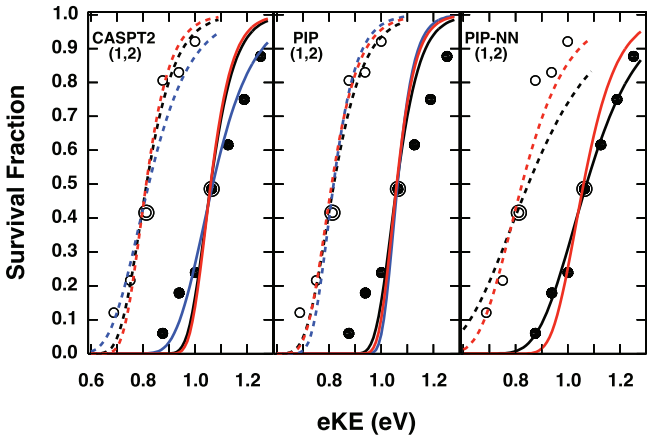

FIG. 9. As in Fig. 8 only for isotope-specific optimized values of χ. See text for details.

for ν_{max} = (1,2) the results in Fig. 9 for the CASPT2, PIP, and PIP-NN PESs. (In Fig. 9 for PIP-NN, the qualitatively incorrect Eckart results have been removed.) Each panel in this figure can be compared to the appropriate panel (c) in Figs. 6–8. The two large circles in each panel of Fig. 9 highlight for each isotope the measurement survival fraction closest to 0.5. As can be seen from Fig. 9, all computed survival fractions pass quite near these two measurements, something that is not the case in Figs. 6–8. This is the primary change of allowing isotopically different values of χ for *all* panels of Figs 6–8 with the exception of the Eckart results on the PIP-NN PES in Fig. 8. Only results for ν_{max} = (1,2) are shown in Fig. 9 because this value of ν_{max} remains the one where experiment and theory most agree. That agreement is an improvement over that in the earlier figures, especially for the PIP PES. All of the results in Fig. 9 are in reasonable agreement with experiment with the Eckart results for CASPT2 and the SCT or iSCTST results for PIP-NN remaining in best agreement. The variations in χ for the results in Fig. 9 are listed in Table II. The results in Table I for for ν_{max} = (1,2) are the approximate average of the results in Table II. For CASPT2 and PIP-NN, the isotopic differences for each tunneling method are quite modest at 0.1 or less with the HOCO value being larger. For PIP, the isotopic differences are about twice as big at 0.2 or less with again HOCO being larger. Table II and Fig. 9 give a lower bound to the product CO_2 internal energy of ∼0.1 eV for both isotopes for CASPT2 and PIP and

TABLE II. Optimized values of isotopically different χ as a function of the tunneling method and the PES, for initial vibrational state quantum numbers ν_{max} = (1,2).

PES	isotope	SCT	Eckart	iSCTST
CASPT2	HOCO	0.40	0.26	0.45
	DOCO	0.30	0.22	0.35
PIP	HOCO	0.42	0.54	0.49
	DOCO	0.28	0.34	0.30
PIP-NN	HOCO	0.18		0.28
	DOCO	0.12		0.18

~0.2 eV for both isotopes for PIP-NN. All of these values are reasonably consistent with experiment.

V. SUMMARY

The measured H(D)OCO survival fractions by the photoelectron-photofragment coincidence experiments by the Continetti group have been qualitatively reproduced by tunneling calculations on several recent *ab initio* potential energy surfaces for the HOCO system. The tunneling calculations were not full dimensional quantum dynamics calculations that are not feasible at this time. Rather they are tunneling calculations through effective 1D barriers based on steepest descent paths computed on each potential energy surface. The resulting tunneling probabilities are converted into H(D)OCO survival fractions using a model developed by the Continetti group in which every oscillation of the H(D)-OCO stretch provides an opportunity to tunnel with an energy equal to the energy in the H(D)-OCO stretch plus an adjustable fraction of the energy available in all the other degrees of freedom. Best agreement with experiment occurs for the maximum amount of energy in the stretch [$v = 1(2)$ for H(D)OCO] and a modest fraction of 0.2–0.4 depending on the tunneling method and the potential energy surface. Similar results were found by the Continetti group using an adjustable potential that could be made to quantitatively represent the measured survival fractions.

Of the four potential energy surfaces investigated, the most recently published potential energy surface based on a permutational invariant polynomial neural network fit to CCSD(T)-F12a/AVTZ electronic structure calculations overall best represented the measured survival fractions. This surface has a larger *ab initio* data set and a more accurate fit to the data set than the PIP surface which did not do quite as well. A partial potential energy surface was constructed for this study based on CASPT2/AVDZ electronic structure calculations. This surface has a higher barrier by 1.6 kcal/mol than the neural network surface but a very similar shape. The higher barrier can be partially compensated for by a higher adjustable fraction of the non-stretch energy contributing to tunneling, resulting in computed survival fractions that are overall the second best representation of the measured values. The fourth and oldest surface tried is the LTSH surface based on a variety of electronic structure calculations done for relatively small numbers of HOCO geometries. This surface has a small discontinuity that had to be repaired for this application but the computed survival probabilities are in qualitative *dis*agreement with the measurements.

On each surface, four different approximate tunneling methods were tried. Two of those methods qualitatively failed on at least one surface. These two methods used the least information about the tunneling path. The Eckart tunneling method, which only uses the barrier from both directions and the imaginary frequency, produces too high a tunneling probability on the neural network surface, leading to survival fractions that peaked out at ~0.5 rather than the measured values of near 1.0. The semiclassical transition state theory method embodied in the Multiwell suite of codes uses an up to quartic description of the saddle point region but no direct information about the barriers. This method produced qualitatively incorrect tunneling probabilities (essentially undefined probabilities) on all the surfaces except the PIP surface. The two remaining methods worked on all the surfaces and produced survival fractions fairly close to each other. One of these methods is the extensively used small curvature method embodied in POLYRATE that explicitly uses all of the reaction path calculated at a harmonic level. The second method is a recently developed *improved* semiclassical transition state theory method that uses all the saddle point information of the original method and also the values of the barriers. This application is one of the first for this improved method that has previously only been applied to model problems. The two successful methods operationally trade off the electronic structure expense of calculating a reaction path at a harmonic level versus characterizing the saddle point up to a partial quartic level.

There are many approximations in the calculations that have been described in this article. Nonetheless, they show that the measurements are supported by calculations using the most recent potential energy surfaces and using tunneling methods that use the most information from those surfaces. The measurements are capable of distinguishing different tunneling methods on the same potential energy surface. The approach used here can be applied to other systems and other experiments where deep tunneling through barriers is probed.

ACKNOWLEDGMENTS

This material is based upon work supported by the U.S. Department of Energy, Office of Science, Office of Basic Energy Sciences, Division of Chemical Sciences under Contract No. DE-AC02-06CH11357 (A.F.W.) and Award Nos. DE-SC0010616 (R.D.), DE-FG03-98ER14879 (R.E.C.), and DE-FG02-05ER15694 (H.G.).

[1] J. A. Miller, R. J. Kee, and C. K. Westbrook, Annu. Rev. Phys. Chem. **41**, 345 (1990).
[2] B. J. Finlayson-Pitts and J. N. Pitts, Jr., *Chemistry of the Upper and Lower Atmosphere* (Academic Press, San Diego, CA, 2000).
[3] Y. L. Yung and W. B. DeMore, *Photochemistry of Planetary Atmospheres* (Oxford University Press, Oxford, UK, 1999).
[4] J. S. Francisco, J. T. Muckerman, and H.-G. Yu, Acc. Chem. Res. **43**, 1519 (2010).
[5] D. Fulle, H. Hamann, H. Hippler, and J. Troe, J. Chem. Phys. **105**, 983 (1996).
[6] H. Guo, Int. Rev. Phys. Chem. **31**, 1 (2012).
[7] T. Sears, W. Fawzy, and P. Johnson, J. Chem. Phys. **97**, 3996 (1992).
[8] J. Petty and C. Moore, J. Mol. Spectrosc. **161**, 149 (1993).
[9] D. Forney, M. Jacox, and W. Thompson, J. Chem. Phys. **119**, 10814 (2003).
[10] D. Milligan and M. Jacox, J. Chem. Phys. **54**, 927 (1971).
[11] T. Oyama, W. Funato, Y. Sumiyoshi, and Y. Y. Endo, in 65th OSU International Symposium on Molecular Spectroscopy, Columbus, OH, 2010.
[12] J. Petty and C. Moore, J. Chem. Phys. **99**, 47 (1993).
[13] M. Jacox, J. Chem. Phys. **88**, 4598 (1988).
[14] C. J. Johnson and R. E. Continetti, J. Phys. Chem. Lett. **1**, 1895 (2010).
[15] C. J. Johnson, M. E. Harding, B. L. J. Poad, J. F. Stanton, and R. E. Continetti, J. Am. Chem. Soc. **133**, 19606 (2011).
[16] C. J. Johnson, B. L. J. Poad, B. B. Shen, and R. E. Continetti, J. Chem. Phys. **134**, 171106 (2011) with supplementary material at http://dx.doi.org/10.1063/1.3589860.
[17] G. C. Schatz, M. S. Fitzcharles, and L. B. Harding, Faraday Discuss. Chem. Soc. **84**, 359 (1987).

[18]H.-G. Yu, J. T. Muckerman, and T. J. Sears, Chem. Phys. Lett. **349**, 547 (2001).
[19]M. J. Lakin, D. Troya, G. C. Schatz, and L. B. Harding, J. Chem. Phys. **119**, 5848 (2003).
[20]R. Valero, M. C. Van Hemert, and G.-J. Kroes, Chem. Phys. Lett. **393**, 236 (2004).
[21]J. Li, Y. Wang, B. Jiang, J. Ma, R. Dawes, D. Xie, J. M. Bowman, and H. Guo, J. Chem. Phys. **136**, 041103 (2012).
[22]C. Xie, J. Li, D. Xie, and H. Guo, J. Chem. Phys. **137**, 024308 (2012).
[23]J. Chen, X. Xu, X. Xu, and D. H. Zhang, J. Chem. Phys. **138**, 221104 (2013).
[24]J. Li, J. Chen, D. H. Zhang, and H. Guo, J. Chem. Phys. **140**, 044327 (2014).
[25]J. Ma, J. Li, and H. Guo, Phys. Rev. Lett. **109**, 063202 (2012).
[26]J. Li, C. Xie, J. Ma, Y. Wang, R. Dawes, D. Xie, J. M. Bowman, and H. Guo, J. Phys. Chem. A **116**, 5057 (2012).
[27]J. C. Corchado, J. Espinos-Garcia, J. Li, and H. Guo, J. Phys. Chem. A **117**, 11648 (2013).
[28]J. Ma, J. Li, and H. Guo, J. Phys. Chem. Lett. **3**, 2482–2486 (2012).
[29]J. Wang, J. Li, J. Ma, and H. Guo, J. Chem. Phys., **140**, 184314 (2014).
[30]T. Shiozaki, W. Gyorffy, P. Celani, and H.-J. Werner, J. Chem. Phys. **135**, 081106 (2011).
[31]C. Eckart, Phys. Rev. **35**, 1303 (1930).
[32]J. Zheng, S. Zhang, B. J. Lynch, J. C. Corchado, Y.-Y. Chuang, P. L. Fast, W.-P. Hu, Y.-P. Liu, G. C. Lynch, K. A. Nguyen, C. F. Jackels, A. Fernandez Ramos, B. A. Ellingson, V. S. Melissas, J. Villà, I. Rossi, E. L. Coitiño, J. Pu, T. V. Albu, R. Steckler, B. C. Garrett, A. D. Isaacson, and D. G. Truhlar, POLYRATE–Version 2010, University of Minnesota, Minneapolis, 2010, see http://comp.chem.umn.edu/polyrate/.
[33]W. H. Miller, R. Hernandez, N. C. Handy, D. Jayatilaka, and A. Willets, Chem. Phys. Lett. **172**, 62 (1990).
[34]T. L. Nguyen, J. F. Stanton, and J. R. Barker, Chem. Phys. Lett. **499**, 9 (2010); J. Phys. Chem. A **115**, 5118 (2011).
[35]A. F. Wagner, J. Phys. Chem. A **117**, 13089 (2013).
[36]E. Wigner, Phys. Rev. **40**, 749 (1932).
[37]See http://www.theory.northwestern.edu/schatz/codes/codes.html for the LTSH code.
[38]T. B. Adler, G. Knizia, and H.-J. Werner, J. Chem. Phys. **127**, 221106 (2007).
[39]G. Knizia, T. B. Adler, and H.-J. Werner, J. Chem. Phys. **130**, 054104 (2009).
[40]B. J. Braams and J. M. Bowman, Int. Rev. Phys. Chem. **28**, 577 (2009).
[41]B. Jiang and H. Guo, J. Chem. Phys. **139**, 054112 (2013).
[42]J. Li, B. Jiang, and H. Guo, J. Chem. Phys. **139**, 204103 (2013).
[43]X. Wang and J. M. Bowman, J. Phys. Chem. A **118**, 684 (2014). This reference outlines a significantly different way of representing the alignment of HOCO normal modes with the tunneling direction. It uses a one-dimensional tunneling path qualitatively similar to that in Fig. 3 for the PIP-NN. The reference does not report the energies at which the tunneling probabilities listed in its Table II were calculated, but Fig. 1 of the reference graphically indicates an energy of ∼9.1 kcal/mol for the OH stretch $v = 1$ tunneling probability of 3.67×10^{-14} in Table 2 of the reference. This energy is below the energies listed in Fig. 3 of this paper. SCT and iSCTST tunneling probabilities on the PIP-NN PES would be about ∼40 time lower than this result. Considering how small the tunneling probability is and that the PESs and the reaction path are different, this is reasonable agreement between two different approaches. Indeed, recent full dimensional calculations (Ref. 29) indicated that the 1D model significantly overestimates the lifetime of low-lying resonances.
[44]T. J. Lee, Chem. Phys. Lett. **372**, 362 (2003).
[45]K. Klein, E. Garand, T. Ichino, D. M. Neumark, J. Gauss, and J. F. Stanton, Theor. Chem. Acc. **129**, 527 (2011).
[46]H.-J. Werner, P. J. Knowles, G. Knizia, F. R. Manby, and M. Schütz, WIREs Comput. Mol. Sci. **2**, 242 (2012), see http://www.molpro.net.
[47]A modification by A. W. Jasper of GAUSSRATE 2009-A by J. Zheng, S. Zhang, J. C. Corchado, Y.-Y. Chuang, E. L. Coitiño, B. A. Ellingson, and D. G. Truhlar, Department of Chemistry and Supercomputing Institute, University of Minnesota, Minneapolis, MN 55455-0431, USA.
[48]B. Ruscic, Active Thermochemical Tables, Version 1.110, see http://atct.anl.gov.
[49]In Ref. 16, there is discussion and a plot (Fig. 3) of an *ab initio* minimum energy barrier derived by a fully relaxed, zero-pointed corrected scan of the energy along the OH bond length. The tunneling path developed by this method and indicated in Fig. 3 of Ref. 16 is *not* equivalent to the steepest descent path used to construct Fig. 2 in this article. The steepest descent path will follow the floor of the valley on the PES that leads to either reactants or products, unlike the path displayed in Fig. 3 of Ref. 16.
[50]B. A. Ruf and W. H. Miller, J. Chem. Soc., Faraday Trans. 2 **84**, 1523 (1988) (see appendix).
[51]See supplementary material at http://dx.doi.org/10.1063/1.4891675 for details of PES features and implementation details of the model and tunneling methods.